

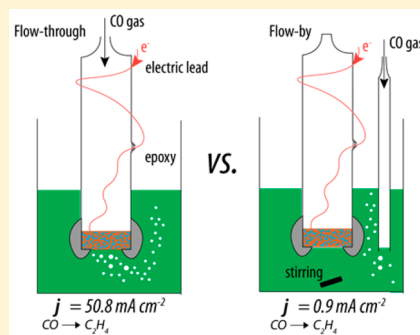
High-Rate Electrochemical Reduction of Carbon Monoxide to Ethylene Using Cu-Nanoparticle-Based Gas Diffusion Electrodes

Lihao Han,¹ Wu Zhou, and Chengxiang Xiang*

Joint Center for Artificial Photosynthesis, and Division of Chemistry and Chemical Engineering, California Institute of Technology, Pasadena, California 91125, United States

S Supporting Information

ABSTRACT: Gas diffusion electrodes (GDEs) with high electrochemically active surface areas (ECSAs) and triple-phase boundaries for efficient gas, electron, and ion transport offer a unique opportunity for high-rate electrochemical CO reduction (COR) in relative to traditional aqueous configurations. Cu-nanoparticle-based GDEs were fabricated by applying a mixture of carbon powders, copper acetate aqueous solution, and Teflon onto a Cu gauze substrate. The catalyst-coated substrate was air-dried, mechanically pressed, and subsequently annealed under forming gas to produce GDEs. Two distinctive types of GDE configurations, a flow-through configuration and a flow-by configuration, were constructed, characterized, and tested to quantitatively evaluate the effects of reactant gas transport on the activity and the selectivity of the GDE materials for COR. In the flow-through configuration, a high partial current density of 50.8 mA cm^{-2} for COR to C_2H_4 was achieved at -0.85 V vs RHE in 10 M KOH at $-15 \text{ }^\circ\text{C}$, while in the flow-by configuration with the same catalyst materials the partial current density for C_2H_4 generation was limited to $<1 \text{ mA cm}^{-2}$.



Utilizing solar energy to transform carbon dioxide (CO_2) into value-added fuels has the potential to reduce the greenhouse gas (GHG) emission and to produce sustainable fuels at large scale. Electrochemical reduction of CO_2 is one of the promising approaches with near-room-temperature operation and mild reaction conditions,^{1–9} however, significant challenges remain in discovering new catalyst materials and understanding fundamental reaction mechanisms for the multielectron and multiproton coupled reactions. Efficient, selective, and stable electrocatalysts for CO_2 reduction (CO_2R) that involves more than two electrons and two protons, such as methanol, ethylene (C_2H_4), and ethanol, have yet to be identified. In contrast to the poor selectivity for the higher-order reduction products, many catalyst systems demonstrated efficient and selective CO_2R to carbon monoxide (CO) or formate.^{10,11} For instance, high Faraday efficiency (FE) and high reaction rates were reported for CO_2R to CO in nanostructured metal dichalcogenides¹² and silver electrodes¹³ in ionic liquids. Near-unity FE for electrochemical CO_2R to formate at an operating current density of $\sim 10 \text{ mA cm}^{-2}$ was also demonstrated in Pd/C nanoparticle-based electrodes.¹⁴ Hence, one alternative strategy for efficient CO_2R is to use a tandem reactor: the first catalytic reactor efficiently and selectively converts CO_2 into CO or formate, and the second catalytic reactor converts CO or formate into higher-order reduction products, such as methane, ethylene, and ethanol.

One advantage of using the tandem strategy is that each reactor can be optimized individually in terms of electrocatalysts, electrolytes, and membrane separators. For instance, high-pH solutions are preferred electrolytes for both CO_2R and carbon monoxide reduction (COR) due to suppression of the hydrogen evolution reaction (HER). However, because of the acid–base equilibrium of CO_2 in the solution, the concentration of dissolved CO_2 at the electrode surface quickly approached zero in high-pH electrolytes,^{15–17} which significantly limited the partial current density for CO_2R . Similarly, when CO_2 was bubbled into high-pH electrolytes in a GDE configuration, the pH of the solution would decrease continuously, and in many cases, the reaction rate between CO_2 and the solution would be much higher than that of the desired electrochemical reduction. As a result, CO_2R in high-pH electrolytes is not a sustainable cathode reaction and would result in very low CO_2 utilization in the reactor. In contrast, COR in alkaline conditions would not have those issues because CO does not react with high-pH electrolytes.

While CO is one of the important intermediate species for CO_2R into hydrocarbons, formate is widely considered as a dead-end product for further reduction.¹⁸ For COR, Cu

Received: January 31, 2018

Accepted: March 13, 2018

Published: March 13, 2018

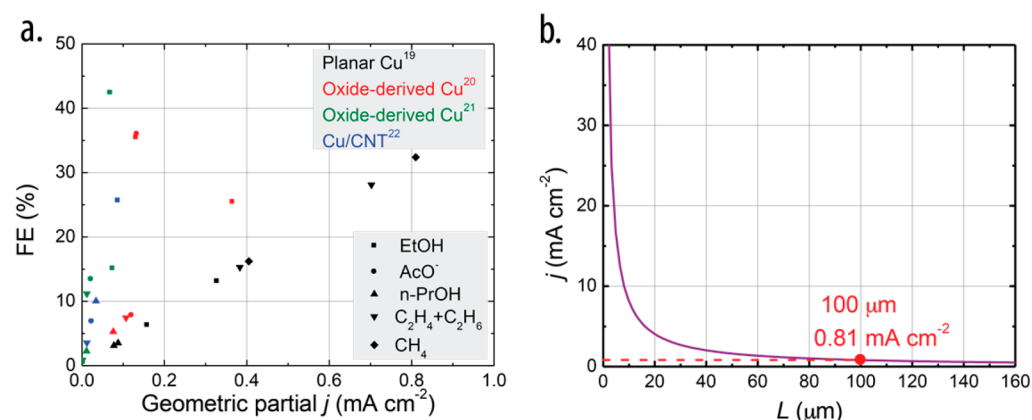


Figure 1. (a) Partial current density vs the FE for COR reported in the literature. (b) Simulated limiting current density for COR to C₂H₄ or C₂H₆O at unity FE as a function of hydrodynamic boundary layer thickness based on Fick's law of diffusion.

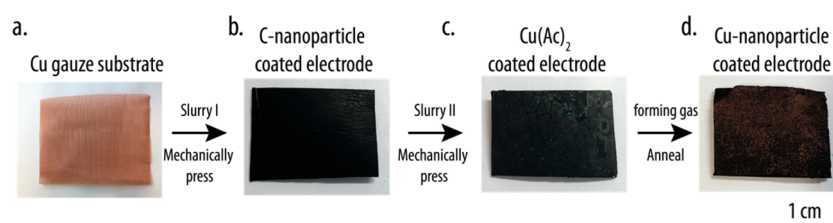


Figure 2. Fabrication process for Cu-nanoparticle-based GDEs: (a) Cu gauze was used as the substrate; (b) Slurry I containing carbon powders, Teflon, and water was applied onto the Cu gauze substrate and mechanically pressed after being dried in air; (c) Slurry II containing carbon powders, Teflon, and copper acetate solution was applied onto the previous layers and mechanically pressed after being dried in air; (d) Cu nanoparticles were formed when the copper acetate in the sample was reduced in forming gas at 325 °C for 7 h.

materials in various forms have been investigated.^{19–22} Figure 1a summarizes the performance of Cu-based materials for COR. Various reduction products, including ethanol, acetoxy, 1-propanol, ethylene, methane, etc., were generated with FEs ranging from 0.49 to 42.42%. While some notable FEs (>40%) for COR were demonstrated, due to the low solubility and low diffusion coefficient of CO in aqueous solution, the geometric partial current densities for COR were limited to <1 mA cm⁻².^{19–22} Figure 1b shows the calculated limiting current density for COR to ethylene or ethanol with unity FE as a function of hydrodynamic boundary layer thickness. Unlike CO₂R in the aqueous solution, in which dissolved CO₂ is replenished from the CO₂/bicarbonate equilibrium during the electrochemical reaction and the local pH and CO₂ concentration at the electrode surface are related to the acid–base equilibrium in the electrolyte,^{15,23,24} COR is much more straightforward as CO does not participate in any electrolyte reactions. The limiting current density for a planar electrode for COR simply follows Fick's law of diffusion (eq 1), in which j is the partial current density, D_0 and C_0 are the diffusion coefficients ($D_0 = 2.1 \times 10^{-9}$ m² s⁻¹ at 20 °C) and the solubility of CO in aqueous solution ($C_0 = 1$ mM at 20 °C), respectively, L is the hydrodynamic boundary layer thickness, n is the number of electrons involved in the COR ($n = 4$ for CO to (1/2)C₂H₄ or (1/2)C₂H₆O), and F is the Faraday constant.

$$j = nFD_0 \frac{C_0}{L} \quad (1)$$

For planar systems at moderate stirring/convection conditions, the mass transport-limited current density was calculated to be ~ 0.81 mA cm⁻² at a boundary layer thickness of ~ 100 μm. It is also noted that microstructured or high-

surface-area catalyst systems in aqueous solutions would have the same transport limitations for the attainable geometric current densities due to the overlap of the diffusion layers extended into the bulk region during operation.²⁵ In order to achieve the geometric partial current density for COR in the tens or hundreds of mA cm⁻² range, an effective boundary layer thickness of <10 μm is required, which is equivalent to the thickness of the hydrodynamic boundary layer in a rotating disk electrode (RDE) at a rotating speed of 7×10^6 rpm.²⁵ As a result, a high partial current density for COR in a planar system is extremely difficult to obtain with traditional aqueous transport approaches. To circumvent the transport limitation of CO, gas diffusion electrodes (GDEs) offer a unique opportunity to achieve high geometric current densities. The concept of a gas/vapor-fed device for electrochemical reaction, such as nitrogen reduction and CO₂R, can be traced back to 1980s.²⁶ Since then, various configurations of GDEs have been employed to obtain high rates for CO₂R reactions in a range of operating pHs and electrolytes.^{26–38} For instance, highly active and stable Sn-based GDEs have been reported for selective formate generation,²⁷ and Cu-based GDEs have shown enhanced selective and activity for CO₂R in mixed solvents.^{26–34} These GDEs are often comprised of nanostructured catalyst materials with extremely high electrochemically active surface areas (ECSAs), and the reactants were directly fed into the electrodes in the gas phase. In general, two distinctive types of GDEs were reported, both of which improved the operating current densities significantly. One type of GDE utilized liquid electrolyte, such as aqueous bicarbonate electrolyte for CO₂R, as the proton source for electrochemical reduction,^{23,28,39} and the other type of GDE directly deposited the catalyst materials onto ion-exchange membranes and

utilized membrane-based electrolyte, such as Nafion, as the proton transport conduct.³⁹

To our knowledge, COR using the GDE configuration to improve the reaction rates has yet to be demonstrated. In this work, Cu-nanoparticle-based GDEs were fabricated, tested, and characterized for COR in alkaline conditions. Two distinctive types of GDE configurations, a flow-through configuration and a flow-by configuration, were constructed, characterized, and compared to quantitatively evaluate the effects of reactant gas transport on the activity and selectivity of the GDE materials. We report a high C_2H_4 partial current density of 50.8 mA cm^{-2} at -0.85 V vs RHE in 10 M KOH at $-15 \text{ }^\circ\text{C}$ in a flow-through GDE configuration.

Figure 2 shows the fabrication process of the Cu-nanoparticle-based GDEs. The GDE fabrication process followed a previously reported recipe.²⁶ Briefly, Slurry I containing C powders, Teflon, and H_2O was applied onto a Cu gauze substrate, air-dried, and then mechanically pressed at 5000 psi (2 min) three times (Figure 2b). Then, Slurry II containing $Cu(Ac)_2$ solution, C powders, and Teflon was applied onto the previous C layers, air-dried, and then mechanically pressed at 1000 psi (2 min) three times, and the black sample with C powders exhibited partly bluish, as presented in Figure 2c. Finally, the catalyst-coated substrate was annealed under the forming gas ($5\% H_2$ in N_2) at $325 \text{ }^\circ\text{C}$ for 7 h. The color of the catalyst-coated substrate changed from partly bluish to brown after the annealing process (Figure 2d). The Cu-nanoparticle-based GDEs have a layer thickness of $\sim 0.1 \text{ mm}$ with a Cu loading of $\sim 7 \text{ mg cm}^{-2}$. The details of the experimental procedure are described in the Supporting Information.

The morphology and chemical composition of the GDEs were characterized by a scanning electron microscope (SEM) and energy-dispersive X-ray spectroscopy (EDX). To obtain the cross-sectional SEM image and to prevent the catalyst powders from peeling off during the characterization, the GDEs were sandwiched between two epoxy layers before slicing the cross section. Figure 3a shows the false-colored cross-sectional

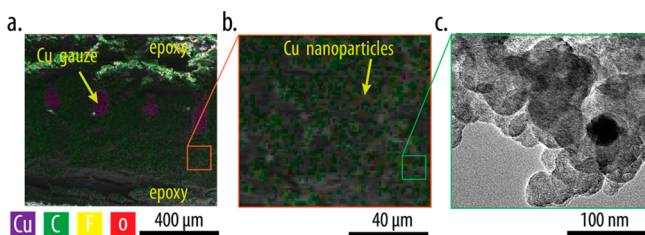


Figure 3. Cross-sectional SEM images with elemental mapping (a,b) and the HR-TEM image (c) of Cu-nanoparticle-based GDEs.

SEM/EDX image of the GDE (the original SEM image is presented in Figure S1a). The C powders (green) were pressed onto the Cu gauze substrate. Cu (purple) was found in the bulk gauze substrate and also in the nanoparticles among the C powders. Figure 3b shows a zoomed-in image of the Cu nanoparticles in the GDEs. During the mechanical pressing and annealing process, the Cu nanoparticles were diffused throughout the carbon layers. High-resolution transmission electron microscopy (HR-TEM) was utilized to characterize the Cu particles that were peeled off from the GDEs. The average size of the Cu nanoparticles in GDEs was $46.56 \pm 4.61 \text{ nm}$ (Figure 3c). By further analyzing the HR-TEM images (Figure S1b), the distance between each lattice was determined

to be 0.26 nm , which agreed well with the lattice constant of Cu material as a typical face-centered cubic system.

Two types of electrode configurations, a flow-through GDE configuration and a flow-by GDE configuration, were fabricated with the same GDE materials to quantitatively evaluate the effects of CO transport and delivery on the selectivity and activity of electrodes. In the flow-through configuration (Figure 4a), the custom-made GDE materials with a diameter of 6 mm were sealed at the end of a glass tube with epoxy. All of the GDEs measured in this study had a geometric surface area of $\sim 0.3 \text{ cm}^2$. The electrical connections to the GDE materials were made by welding a flexible Cu wire to the Cu gauze substrate. The flexible Cu wire was weaved through the sidewall of the glass tube, while CO gas was introduced directly from the top of the glass tube. In the flow-by configuration (Figure 4b), the previous gas inlet at the end of the glass tube was sealed with epoxy, and the CO gas was injected from the side inlet along with rapid stirring to provide fresh CO-saturated electrolyte flowing by the GDE surface. Figure 4c shows the cyclic voltammetry of both electrode configurations from 0 to -0.9 V vs RHE (from -0.8 to -2.4 V vs $Ag/AgCl$ in the experiment) at a scan rate of 40 mV s^{-1} in 10 M KOH . The use of high-concentration KOH aimed to suppress the competing HER in high-pH electrolyte and to lower the solution resistance loss in the electrochemical cells. In addition, a high concentration of KOH ($25\text{--}30 \text{ wt } \%$) is widely adopted in commercial electrolyzers to promote the ionic transport and oxygen evolution reaction (OER) at the anode chamber.^{40,41}

For both configurations, the CO flow rate was set to 20.0 sccm . The whole cell was immersed in a cooling bath, and the temperature was controlled at around $-15 \text{ }^\circ\text{C}$. The uncompensated resistance (R_u) was measured using an IR compensation (PEIS)-ZIR technique in a Biologic SP-300 potentiostat, and the R_u at $-15 \text{ }^\circ\text{C}$ was measured to be $2.27 \text{ } \Omega$. The potentials due to the IR loss in each curve in Figure 4c were compensated, and the curves were smoothed using the Savitzky–Golay method in the fifth polynomial order to reduce the noise in the raw data (Figure S2) due to vigorous CO bubbling. The J – V performances for the flow-through configuration were relatively stable during $\sim 3.5 \text{ h}$ of testing, and the slight increase in the total current density (also see Figure S2a) was likely due to the increase of the ECSAs as part of clogged porous channels in the initial GDEs getting cleared out during the CO bubbling. In contrast, a relatively large increase of the total current density in the flow-by configuration was observed (also see Figure S2b), which was likely due to the continuous increase of the wetted area and the ECSAs after immersing the electrodes in the solution. No visible catalyst loss was observed during the testing period, and both configurations exhibited a similar total operating current density toward the end of the testing.

Figure 5 shows the FE, total operating current density, and partial current density for COR to C_2H_4 as a function of the applied voltage bias vs RHE in 10 M KOH at $-15 \text{ }^\circ\text{C}$. An online gas chromatograph (GC) was connected in the electrochemical system and was calibrated for H_2 and a majority of common hydrocarbon gases (Figure S3). The electrodes for both configurations were poised at each potential for $\sim 40 \text{ min}$, and the gaseous products were detected and analyzed. In the flow-through configuration, a partial current density of 50.8 mA cm^{-2} and a FE of 17.8% for COR to C_2H_4 were achieved at -0.85 and -0.74 V vs RHE, respectively. The observed partial current density for C_2H_4 generation was

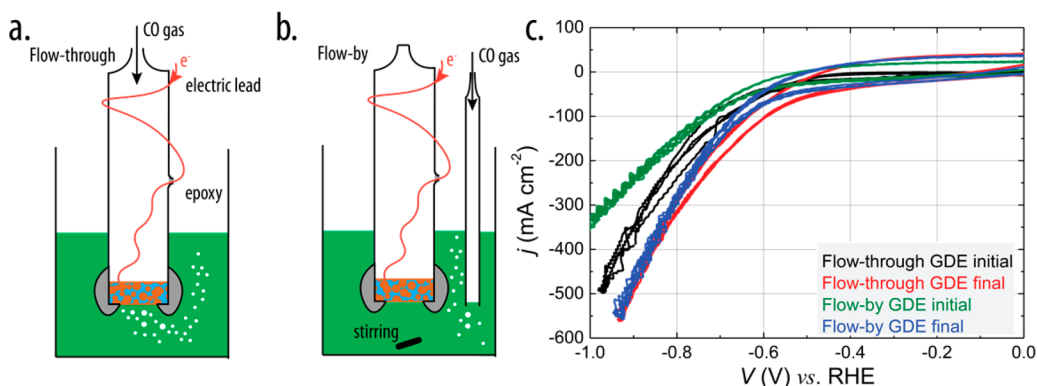


Figure 4. Schematic illustration of the GDE materials in the flow-through configuration (a) and in the flow-by configuration (b). Cyclic voltammetry for both configurations before and after 3.5 h of operation (c).

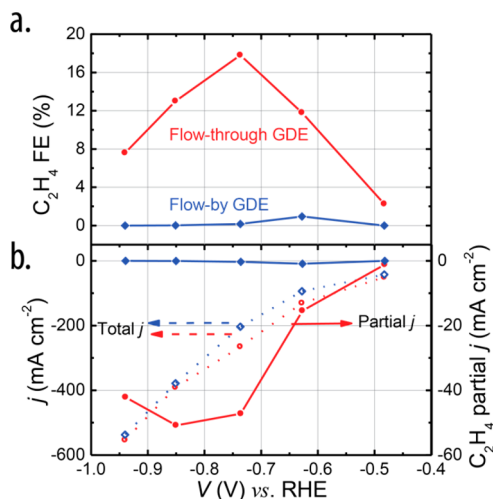


Figure 5. (a) FE for COR to C₂H₄ as a function of the applied potential for the flow-through configuration and the flow-by configuration. (b) Total operating current density (dotted curves, left y-axis) and partial current density for COR to C₂H₄ (solid curves, right y-axis) as a function of applied potential for the flow-through configuration (red) and the flow-by configuration (blue). Both GDE configurations were operated in pH 15 KOH electrolyte at -15 °C, and the potential was compensated by IR drop measurement.

significantly higher than those reported previously.^{19–22} The FE for COR to C₂H₄ peaked at -0.74 V vs RHE (Figure 5a). As the applied potential increased from -0.74 to -0.94 V vs RHE while the total operating current density increased (Figure 5b), the FE for COR to C₂H₄ decreased significantly and the majority of the electrons contributed to HER. Domination of the HER at significantly high potentials was also observed by others for both COR and CO₂R in Cu-based electrocatalysts.^{19,42,43}

In contrast, in the flow-by configuration, the maximum partial current density and the maximum FE for C₂H₄ generation were 0.90 mA cm⁻² and 0.94%, respectively. The low COR current density (<1 mA cm⁻²) in the flow-by configuration agreed well with the Fick's law calculation (Figure 1b). The majority of the reduction product was hydrogen (Figure S4) for both configurations; liquid products from COR, such as ethanol, methanol, and acetaldehyde, were also detected using a Thermo Scientific TRACE 1300 offline GC. However, quantitative FEs for those liquid products were challenging to obtain in the flow-through configuration and were labeled as unknown reduction products.

The high geometric current density and high rate for COR observed in Cu-nanoparticle-based GDEs in the flow-through configuration originated from the high ECSA and efficient gas, electron, and ion transport at triple-phase boundaries. The ECSAs of the GDEs in the flow-through configuration were estimated using double-layer capacitance measurements in 10

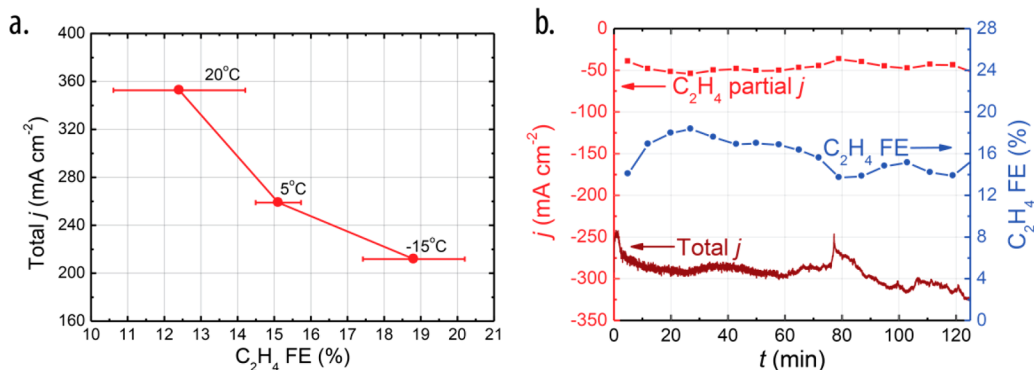


Figure 6. (a) Total operating current density and FE for COR to C₂H₄ for three different operating temperatures when the GDE material in the flow-through configuration was poised at -2.0 V vs Ag/AgCl (the IR-corrected potentials at three different temperatures were quite similar, -0.80 ± 0.02 V vs RHE) in 10 M KOH. (b) Total and C₂H₄ partial current density (left y-axis) and FE (right y-axis) of C₂H₄ generation as a function of the operating time when the GDE material in the flow-through configuration was poised at -2.0 V vs Ag/AgCl (-0.78 V vs RHE with IR correction) in 10 M KOH at -15 °C.

M KOH (Figure S5).⁴⁴ The ECSAs of the flow-through configuration decreased gradually from 970 to 674 cm² when the injection CO flow rate increased from 5 to 80 sccm (Figure S6). At higher CO flow rates (>50 sccm), delamination of catalyst materials was observed in several GDE samples, and hence, a moderate flow rate of 20 sccm was chosen for the study. At a flow rate of 20 sccm, the ECSA was determined to be 950 cm², which corresponds to a roughness factor of 3167 (ratio of ECSA and geometric area). The direct gas feed in the flow-through configuration also played a critical role in improving the reaction rates. The flow-through GDE structure contained agglomerate catalyst materials (Cu nanoparticle, C nanoparticle, and polymer binders), microstructured gas channels, and electrolyte channels. During the CO injection, the agglomerate catalysts were covered with a thin layer of electrolyte that was in equilibrium with the gas-phase reactant CO. The thin electrolyte layer, on the order of hundreds of nanometers, provided efficient CO transport from the gas phase to the catalyst surface, while the electrolyte channels provided efficient transport and mixing for the produced hydroxides toward the bulk electrolyte during the electrochemical reaction. In contrast, although the flow-by GDE configuration had a similar ECSA, CO transport in the aqueous solution without direct gas feed limited the reaction rates for COR.

The electrochemical COR in the flow-through GDE configuration was carried out at three different temperatures. Figure 6a shows the total current density and the corresponding FE for COR to C₂H₄ at three operating temperatures when the GDE was biased at -2.0 V vs Ag/AgCl. The R_i was 2.27, 1.28, and 1.11 Ω; therefore, the IR-corrected applied bias was -0.78, -0.82, and -0.80 V vs RHE at -15, 5, and 20 °C, respectively. The total current density decreased from 353 ± 9 to 212 ± 6 mA cm⁻², while the FE for C₂H₄ generation increased from 12.41 ± 1.8 to 18.81 ± 1.4% when the operating temperature of the cell decreased from 20 to -15 °C. The total operating current density decreased significantly at low temperatures due to the activities of Cu-nanoparticle-based GDE materials for HER, and COR decayed exponentially as a function of the operating temperature. The reduced-temperature operation in the flow-through GDE cell preferentially suppressed HER relative to COR, which resulted in a slight increase of FE for C₂H₄ generation. The stability of the Cu-nanoparticle-based GDEs operating at high rates was also investigated. Figure 6b shows the total and partial current density and the FE for C₂H₄ generation as a function of the operating time when the GDEs in the flow-through configuration were poised at -0.78 V vs RHE electrode in 10 M KOH at -15 °C. The C₂H₄ partial current density was stabilized in the range of 36.8–54.3 mA cm⁻², and the FE for C₂H₄ generation was stabilized between 13.7 and 18.4% during the first 2 h of operation.

In summary, a multistep fabrication process was developed to produce Cu-nanoparticle-based GDEs. Two distinctive types of GDE configurations, a flow-through configuration and a flow-by configuration, were constructed, characterized, and tested to quantitatively evaluate the effects of reactant gas transport on the activity and the selectivity of the catalyst materials. In a flow-through GDE configuration, a high partial current density of 50.8 mA cm⁻² and a FE of 17.8% for COR to C₂H₄ were achieved at -0.85 and -0.74 V vs RHE in 10 M KOH, respectively. The high ECSAs, direct gas feed configuration, and triple-phase boundaries for efficient gas, electron, and ion

transport significantly enhanced the reaction rates of the catalyst materials for COR. In contrast, when the same catalyst materials were constructed in a flow-by GDE configuration, the partial current density for COR to C₂H₄ was limited to <1 mA cm⁻² due to the low solubility and diffusion coefficient of CO in aqueous solution. Direct gas feed configurations provided a unique electrode structure for efficient and stable electrochemical reactions without mass transport limitations, especially for gases with low solubility in aqueous solutions, such as CO, CO₂, and N₂.

■ ASSOCIATED CONTENT

📄 Supporting Information

The Supporting Information is available free of charge on the ACS Publications website at DOI: 10.1021/acseenergylett.8b00164.

GDE fabrication procedures, GDE material characterization details, additional SEM and TEM images, cyclic voltammetry for flow-through and flow-by configurations, GC measurement optimization and calibration, calculation methods of FE, and the ECSA measurement method and results (PDF)

■ AUTHOR INFORMATION

Corresponding Author

*E-mail: cxx@caltech.edu.

ORCID

Lihao Han: 0000-0002-0452-3381

Notes

The authors declare no competing financial interest.

■ ACKNOWLEDGMENTS

This material is based on work performed by the Joint Center for Artificial Photosynthesis, a DOE Energy Innovation Hub, supported through the Office of Science of the U.S. Department of Energy under Award Number DE-SC0004993. The authors also acknowledge experimental assistance from Xinghao Zhou, Dr. Hsiang-Yun Chen, Dr. Yungchieh Lai, and Dr. Bruce S. Brunschwig.

■ REFERENCES

- (1) Gattrell, M.; Gupta, N.; Co, A. A Review of the Aqueous Electrochemical Reduction of CO₂ to Hydrocarbons at Copper. *J. Electroanal. Chem.* **2006**, *594*, 1–19.
- (2) Ye, S.; Wang, R.; Wu, M.-Z.; Yuan, Y.-P. A Review on G-C₃N₄ for Photocatalytic Water Splitting and CO₂ Reduction. *Appl. Surf. Sci.* **2015**, *358*, 15–27.
- (3) Li, C. W.; Kanan, M. W. CO₂ Reduction at Low Overpotential on Cu Electrodes Resulting from the Reduction of Thick Cu₂O Films. *J. Am. Chem. Soc.* **2012**, *134*, 7231–7234.
- (4) Lu, Q.; Rosen, J.; Zhou, Y.; Hutchings, G. S.; Kimmel, Y. C.; Chen, J. G.; Jiao, F. A Selective and Efficient Electrocatalyst for Carbon Dioxide Reduction. *Nat. Commun.* **2014**, *5*, 3242.
- (5) Adachi, K.; Ohta, K.; Mizuno, T. Photocatalytic Reduction of Carbon Dioxide to Hydrocarbon Using Copper-Loaded Titanium Dioxide. *Sol. Energy* **1994**, *53*, 187–190.
- (6) Roberts, F. S.; Kuhl, K. P.; Nilsson, A. High Selectivity for Ethylene from Carbon Dioxide Reduction over Copper Nanocube Electrocatalysts. *Angew. Chem.* **2015**, *127*, S268–S271.
- (7) Mistry, H.; Varela, A. S.; Bonifacio, C. S.; Zegkinoglou, I.; Sinev, I.; Choi, Y.-W.; Kisslinger, K.; Stach, E. A.; Yang, J. C.; Strasser, P.; Cuenya, B. R. Highly Selective Plasma-Activated Copper Catalysts for Carbon Dioxide Reduction to Ethylene. *Nat. Commun.* **2016**, *7*, 12123.

- (8) Asadi, M.; Kumar, B.; Behranginia, A.; Rosen, B. A.; Baskin, A.; Reppin, N.; Pisasale, D.; Phillips, P.; Zhu, W.; Haasch, R.; et al. Robust Carbon Dioxide Reduction on Molybdenum Disulphide Edges. *Nat. Commun.* **2014**, *5*, 4470.
- (9) Cook, R. L.; MacDuff, R. C.; Sammells, A. F. On the Electrochemical Reduction of Carbon Dioxide at In Situ Electrodeposited Copper. *J. Electrochem. Soc.* **1988**, *135*, 1320–1326.
- (10) Jovanov, Z. P.; Hansen, H. A.; Varela, A. S.; Malacrida, P.; Peterson, A. A.; Nørskov, J. K.; Stephens, I. E. L.; Chorkendorff, I. Opportunities and Challenges in the Electrocatalysis of CO₂ and CO Reduction Using Bifunctional Surfaces: A Theoretical and Experimental Study of Au–Cd Alloys. *J. Catal.* **2016**, *343*, 215–231.
- (11) Jhong, H.-R.; Ma, S.; Kenis, P. J. Electrochemical Conversion of CO₂ to Useful Chemicals: Current Status, Remaining Challenges, and Future Opportunities. *Curr. Opin. Chem. Eng.* **2013**, *2*, 191–199.
- (12) Asadi, M.; Kim, K.; Liu, C.; Addepalli, A. V.; Abbasi, P.; Yasaei, P.; Phillips, P.; Behranginia, A.; Cerrato, J. M.; Haasch, R.; et al. Nanostructured Transition Metal Dichalcogenide Electrocatalysts for CO₂ Reduction in Ionic Liquid. *Science* **2016**, *353*, 467.
- (13) Rosen, B. A.; Salehi-Khojin, A.; Thorson, M. R.; Zhu, W.; Whipple, D. T.; Kenis, P. J. A.; Masel, R. I. Ionic Liquid-Mediated Selective Conversion of CO₂ to CO at Low Overpotentials. *Science* **2011**, *334*, 643–644.
- (14) Zhou, X.; Liu, R.; Sun, K.; Chen, Y.; Verlage, E.; Francis, S. A.; Lewis, N. S.; Xiang, C. Solar-Driven Reduction of 1 Atm of CO₂ to Formate at 10% Energy-Conversion Efficiency by Use of a TiO₂-Protected III–V Tandem Photoanode in Conjunction with a Bipolar Membrane and a Pd/C Cathode. *ACS Energy Lett.* **2016**, *1*, 764–770.
- (15) Chen, Y.; Lewis, N. S.; Xiang, C. Modeling and Simulation of the Spatial and Light-Intensity Dependence of Product Distributions in an Integrated Photoelectrochemical CO₂ Reduction System. *ACS Energy Lett.* **2016**, *1*, 273–280.
- (16) Hashiba, H.; Weng, L.-C.; Chen, Y.; Sato, H. K.; Yotsuhashi, S.; Xiang, C.; Weber, A. Z. Effects of Electrolyte Buffer Capacity on Surface Reactant Species and the Reaction Rate of CO₂ in Electrochemical CO₂ Reduction. *J. Phys. Chem. C* **2018**, *122*, 3719–3726.
- (17) Singh, M. R.; Clark, E. L.; Bell, A. T. Effects of Electrolyte, Catalyst, and Membrane Composition and Operating Conditions on the Performance of Solar-Driven Electrochemical Reduction of Carbon Dioxide. *Phys. Chem. Chem. Phys.* **2015**, *17*, 18924–18936.
- (18) Kortlever, R.; Shen, J.; Schouten, K. J. P.; Calle-Vallejo, F.; Koper, M. T. M. Catalysts and Reaction Pathways for the Electrochemical Reduction of Carbon Dioxide. *J. Phys. Chem. Lett.* **2015**, *6*, 4073–4082.
- (19) Hori, Y.; Takahashi, R.; Yoshinami, Y.; Murata, A. Electrochemical Reduction of CO at a Copper Electrode. *J. Phys. Chem. B* **1997**, *101*, 7075–7081.
- (20) Feng, X.; Jiang, K.; Fan, S.; Kanan, M. W. A Direct Grain-Boundary-Activity Correlation for CO Electroreduction on Cu Nanoparticles. *ACS Cent. Sci.* **2016**, *2*, 169–174.
- (21) Li, C. W.; Ciston, J.; Kanan, M. W. Electroreduction of Carbon Monoxide to Liquid Fuel on Oxide-Derived Nanocrystalline Copper. *Nature* **2014**, *508*, 504.
- (22) Verdager-Casadevall, A.; Li, C. W.; Johansson, T. P.; Scott, S. B.; McKeown, J. T.; Kumar, M.; Stephens, I. E. L.; Kanan, M. W.; Chorkendorff, I. Probing the Active Surface Sites for CO Reduction on Oxide-Derived Copper Electrocatalysts. *J. Am. Chem. Soc.* **2015**, *137*, 9808–9811.
- (23) Wu, K.; Birgersson, E.; Kim, B.; Kenis, P. J. A.; Karimi, I. A. Modeling and Experimental Validation of Electrochemical Reduction of CO₂ to CO in a Microfluidic Cell. *J. Electrochem. Soc.* **2015**, *162*, F23–F32.
- (24) Gupta, N.; Gattrell, M.; MacDougall, B. Calculation for the Cathode Surface Concentrations in the Electrochemical Reduction of CO₂ in KHCO₃ Solutions. *J. Appl. Electrochem.* **2006**, *36*, 161–172.
- (25) Bard, A. J.; Inzelt, G.; Scholz, F. *Electrochemical Dictionary*, 2nd ed.; Wiley: New York, 2002.
- (26) Cook, R. L.; MacDuff, R. C.; Sammells, A. F. High Rate Gas Phase CO₂ Reduction to Ethylene and Methane Using Gas Diffusion Electrodes. *J. Electrochem. Soc.* **1990**, *137*, 607–608.
- (27) Kopljar, D.; Inan, A.; Vindayer, P.; Wagner, N.; Klemm, E. Electrochemical Reduction of CO₂ to Formate at High Current Density Using Gas Diffusion Electrodes. *J. Appl. Electrochem.* **2014**, *44*, 1107–1116.
- (28) Ogura, K.; Oohara, R.; Kudo, Y. Reduction of CO₂ to Ethylene at Three-Phase Interface Effects of Electrode Substrate and Catalytic Coating. *J. Electrochem. Soc.* **2005**, *152*, D213–D219.
- (29) Ogura, K.; Endo, N. Electrochemical Reduction of CO₂ with a Functional Gas-Diffusion Electrode in Aqueous Solutions with and without Propylene Carbonate. *J. Electrochem. Soc.* **1999**, *146*, 3736–3740.
- (30) Ogura, K.; Yano, H.; Shirai, F. Catalytic Reduction of CO₂ to Ethylene by Electrolysis at a Three-Phase Interface. *J. Electrochem. Soc.* **2003**, *150*, D163–D168.
- (31) Yano, H.; Shirai, F.; Nakayama, M.; Ogura, K. Efficient Electrochemical Conversion of CO₂ to CO, C₂H₄ and CH₄ at a Three-Phase Interface on a Cu Net Electrode in Acidic Solution. *J. Electroanal. Chem.* **2002**, *519*, 93–100.
- (32) Kim, B.; Ma, S.; Molly Jhong, H.-R.; Kenis, P. J. A. Influence of Dilute Feed and PH on Electrochemical Reduction of CO₂ to CO on Ag in a Continuous Flow Electrolyzer. *Electrochim. Acta* **2015**, *166*, 271–276.
- (33) Ma, S.; Luo, R.; Moniri, S.; Lan, Y.; Kenis, P. J. A. Efficient Electrochemical Flow System with Improved Anode for the Conversion of CO₂ to CO. *J. Electrochem. Soc.* **2014**, *161*, F1124–F1131.
- (34) Whipple, D. T.; Kenis, P. J. A. Prospects of CO₂ Utilization via Direct Heterogeneous Electrochemical Reduction. *J. Phys. Chem. Lett.* **2010**, *1*, 3451–3458.
- (35) Thorson, M. R.; Siil, K. I.; Kenis, P. J. A. Effect of Cations on the Electrochemical Conversion of CO₂ to CO. *J. Electrochem. Soc.* **2013**, *160*, F69–F74.
- (36) Tornow, C. E.; Thorson, M. R.; Ma, S.; Gewirth, A. A.; Kenis, P. J. A. Nitrogen-Based Catalysts for the Electrochemical Reduction of CO₂ to CO. *J. Am. Chem. Soc.* **2012**, *134*, 19520–19523.
- (37) Ma, S.; Sadakiyo, M.; Luo, R.; Heima, M.; Yamauchi, M.; Kenis, P. J. A. One-Step Electrosynthesis of Ethylene and Ethanol from CO₂ in an Alkaline Electrolyzer. *J. Power Sources* **2016**, *301*, 219–228.
- (38) Hoang, T. T. H.; Ma, S.; Gold, J. I.; Kenis, P. J. A.; Gewirth, A. A. Nanoporous Copper Films by Additive-Controlled Electrodeposition: CO₂ Reduction Catalysis. *ACS Catal.* **2017**, *7*, 3313–3321.
- (39) Prakash, G. K. S.; Viva, F. A.; Olah, G. A. Electrochemical Reduction of CO₂ over Sn-Nafion® Coated Electrode for a Fuel-Cell-like Device. *J. Power Sources* **2013**, *223*, 68–73.
- (40) Gutmann, F.; Murphy, O. J. *Modern Aspects of Electrochemistry*; Plenum Press: New York, 1983.
- (41) Zeng, K.; Zhang, D. Recent Progress in Alkaline Water Electrolysis for Hydrogen Production and Applications. *Prog. Energy Combust. Sci.* **2010**, *36*, 307–326.
- (42) Kuhl, K. P.; Cave, E. R.; Abram, D. N.; Jaramillo, T. F. New Insights into the Electrochemical Reduction of Carbon Dioxide on Metallic Copper Surfaces. *Energy Environ. Sci.* **2012**, *5*, 7050–7059.
- (43) Hori, Y.; Kikuchi, K.; Suzuki, S. Production of CO and CH₄ in Electrochemical Reduction of CO₂ at Metal Electrodes in Aqueous Hydrogencarbonate Solution. *Chem. Lett.* **1985**, *14*, 1695–1698.
- (44) McCrory, C. C. L.; Jung, S.; Ferrer, I. M.; Chatman, S. M.; Peters, J. C.; Jaramillo, T. F. Benchmarking Hydrogen Evolving Reaction and Oxygen Evolving Reaction Electrocatalysts for Solar Water Splitting Devices. *J. Am. Chem. Soc.* **2015**, *137*, 4347–4357.